Vibrational Sum Frequency Spectroscopy and Molecular Dynamics Simulation of the Carbon Tetrachloride−Water and 1,2-Dichloroethane−Water Interfaces

Dave S. Walker,[†] Fred G. Moore,[‡] and Geraldine L. Richmond*[,†]

Department of Chemistry, University of Oregon, Eugene, Oregon 97403-1253, and Department of Physics, Whitman College, Walla Walla, Washington 99362-2083

Received: December 18, 2006; In Final Form: February 5, 2007

Vibrational sum frequency (VSF) spectra calculated using molecular dynamics (MD) simulations are compared with VSF experimental spectra to gain a clearer picture of water structure and bonding at the carbon tetrachloride−water (CCl_4-H_2O) and the 1,2-dichloroethane−water (DCE−H_2O) liquid−liquid interfaces. The VSF spectral response from interfacial water at the CCl_4-H_2O interface contains spectral features similar to the resonant VSF response of the vapor−water interface and alkane−water interfaces, while the VSF spectrum from the DCE−H_2O interface has a low signal with no distinguishing OH stretch spectral features. These MD based spectral calculations show how different bonding interactions at the DCE−H_2O interface lead to spectral broadening, frequency shifting, and spectral interferences that are responsible for the difference in the experimentally measured DCE−H_2O and CCl_4-H_2O spectra. The computational results show that weak H_2O-H_2O interactions are perturbed by the presence of DCE, leading to increased water penetration into the more organic-rich portion of the interfacial region and strong orientation of these penetrating water molecules relative to the CCl_4-H_2O interface. Strong H_2O-H_2O interactions at the interface are not significantly impacted by the presence of DCE.

Introduction

The interface between two immiscible liquids provides a unique environment that enables many important chemical and physical processes including polymerization, nanoparticle synthesis, electron transfer, and ion transport. Because of the importance of these processes to such fields as electrochemistry, biophysics, molecular biology, and materials science, much effort has been made to assess how these interfacial processes are affected by the nature and composition of the adjacent aqueous and organic phases. For example, the interface between two immiscible electrolyte solutions (ITIES) has served as an important electrochemical interface for decades, with the 1,2-dichloroethane−water (DCE−H_2O) interface being the most heavily studied. From a fundamental perspective, the liquid−liquid interface has also been considered as a model system for understanding ion and molecular transport across biological membranes, particularly in the theoretical community.[1]

Even with interest from many fields in this complex system, it is only recently that advances in our molecular level understanding have emerged, driven largely by advances in experimental techniques and computational methods. A number of groups have made pivotal contributions to the molecular understanding of a variety of liquid−liquid systems by means of molecular dynamics simulations.[2−9] In the experimental community, vibrational sum frequency (VSF) spectroscopy has emerged as an important method for probing water structure and bonding at a number of liquid−liquid interfaces,[10−16] as well as for measuring the structure and conformation of different surfactants[17−19] and biomolecules[20−22] adsorbed at these interfaces. Schlossman and co-workers have pioneered the use of X-ray scattering techniques to understand the buried alkane−water interface,[23−25] and recently the nitrobenzene−water interface.[26] Eisenthal and co-workers have employed second harmonic generation (SHG) to study the polarity of DCE−H_2O and chlorobenzene−water interfaces.[27] In related studies Walker and co-workers have used SHG in combination with chromophore surfactants that vary in length—so-called "molecular rulers"—to assess how the spectral response varies based on proximity to the interface and interfacial environment.[28−30]

In the VSF studies of the water structure and bonding present at different liquid−liquid interfaces, the system that has shown the most distinct spectral differences to date in the OH stretch region is the 1,2-dichloroethane−water (DCE−H_2O) interface.[13] Unlike the CCl_4-H_2O[31] and the C_6-C_9 alkane−water interfaces,[12] the VSF experimental spectrum of the DCE−H_2O interface gave a low signal in the OH stretch region with none of the distinct spectral features found in these other systems. It was thus concluded[13] that the DCE−H_2O interfacial region was likely more diffuse with water molecules exhibiting more random orientation at this interface relative to the alkane−water and CCl_4-H_2O interfaces. These conclusions were consistent with fluorescence anisotropy experiments[32] and molecular dynamics (MD) simulations[3] that show the DCE−H_2O interface to be wider than the CCl_4-H_2O interface. However, it was recognized that more work was necessary to obtain a detailed explanation for the types of DCE−H_2O and H_2O-H_2O interactions present at the DCE−H_2O interface due to the fact that its spectral response could not be deconvoluted using established curve fitting routines.[33]

In this paper MD simulations are employed as a means of providing detailed descriptions and statistical information pertaining to the structure and bonding of the different water species that contribute to the VSF spectrum of the DCE−H_2O and CCl_4-H_2O interfaces. With the combined efforts of

* To whom correspondence should be addressed. E-mail: richmond@uoregon.edu. Fax: 541-346-5859.
[†] University of Oregon.
[‡] Whitman College.

10.1021/jp068700z CCC: $37.00
Published on Web 03/31/2007

TABLE 1: Nonbonding Parameters for H_2O,[35] CCl_4,[36] and DCE

atom (molecule)	σ (Å)	ϵ (kcal/mol)	q	α
O (H_2O)	3.204	0.1560	−0.7300	0.528
H (H_2O)	0.000	0.0000	0.3650	0.170
C (CCl_4)	3.400	0.1094	−0.1616	0.878
Cl (CCl_4)	3.471	0.2650	0.0404	1.910
C (DCE)	3.400	0.1094	−0.2993	0.878
Cl (DCE)	3.471	0.2650	0.2087	1.910
H (DCE)	2.471	0.0157	0.0453	0.135

experimental and computational approaches directed toward the analysis of the spectral response, a more comprehensive description of water structure is possible. The computational approach deployed herein allows for a detailed deconvolution of the OH stretch region and shows how weakly bonded, highly aligned water species penetrate into the organic phase. From a spectroscopic viewpoint, these interfacial water molecules contribute small quantities of VSF signal that significantly influence the overall spectral line shape via interference effects.[34]

Computational Method

Fully atomistic, polarizable descriptions of molecules were simulated using the AMBER7 suite of programs. A total of 2135 water molecules, 400 carbon tetrachloride (CCl_4) molecules, and 480 1,2-dichloroethane (DCE) molecules were used in separate (40 Å)^3 boxes to reproduce their bulk densities, and each of these boxes was individually equilibrated for 200 ps. Molecular descriptions for POL3 water[35] and CCl_4[36] were readily available within the literature, yet a polarizable description for DCE was more difficult to find until fairly recently.[37] Consequentially, polarizable models from a variety of small halocarbons were used as templates to construct eight different charge configurations for DCE, and each of these configurations was simulated in separate DCE−H_2O systems.[9,35−39] With respect to each model, the water surface remained largely insensitive to these different charge configurations, as these simulations all produced similar results pertaining to interfacial thickness and molecular structure. However, the vibrational frequencies of OH oscillators interacting directly with the organic phase were sensitive to the model of DCE, and the corresponding model that produced the best VSF spectrum of the DCE−H_2O interface was used in this work. The nonbonding parameters for CCl_4, DCE, and POL3 water are shown in Table 1.

Two CCl_4−H_2O interfaces were created by joining together one organic liquid box of (40 Å)^3 with one water box of (40 Å)^3 to produce a periodic cell measuring 80 Å along the *z*-axis. Two DCE−H_2O interfaces were created by joining together two organic liquid boxes and one water box to produce a periodic cell measuring 120 Å along the *z*-axis. (This second organic liquid box was used as a reservoir for individual water molecules within the organic phase.) In all cases, statistics were collected for only the 40 Å × 40 Å × 80 Å region surrounding water and periodic boundaries were applied in all three dimensions. For results dependent upon molecular orientation, one interfacial system was related to the other by means of an inversion operation to ensure the interface normal (positive *z*-axis) was directed toward the organic phase for both interfaces. After a 2 ns equilibration of the liquid−liquid systems, configurations were recorded every 50 fs over the course of the following 3 ns. The time step of integration was 1 fs. The temperature was held at 300 K using weak coupling to a heat bath. The SHAKE algorithm was used to constrain molecular geometries, and the Particle Mesh Ewald technique applied an 8 Å cutoff to handle long-range interactions.

A modified Morita and Hynes (MH) approach[40] was used to evaluate the spectral response of water and has been described in more detail elsewhere,[41] so only a brief description will be provided here. The VSF intensity is proportional to the square of the effective macroscopic susceptibility:

$$I_{SFG} \propto |\chi_{eff}^{(2)}|^2 = |F_{SFG} f_{VIS} f_{IR} (N\langle\beta_{pqr}\rangle + \chi_{NR}^{(2)})|^2 \quad (1)$$

where β_{pqr} is the molecular hyperpolarizability, defined by

$$\beta_{pqr} \approx \frac{1}{2m\omega}\left(\frac{\partial\alpha_{pq}}{\partial Q}\right)\left(\frac{\partial\mu_r}{\partial Q}\right)\left[\frac{\omega - \omega_{IR}}{(\omega - \omega_{IR})^2 + \gamma^2} + \frac{i\gamma}{(\omega - \omega_{IR})^2 + \gamma^2}\right] \quad (2)$$

N is the number of molecules, χ_{NR} is the nonresonant susceptibility, $F_{SFG} f_{VIS} f_{IR}$ is the local field correction, and the derivatives $\partial\mu_r/\partial Q$ and $\partial\alpha_{pq}/\partial Q$ are the infrared transition dipole moment and Raman transition polarizability derivatives, respectively, for an OH normal mode of water with reduced bond mass m and frequency ω in the pqr reference frame. The angled brackets $\langle\ \rangle$ represent an orientation average, which is the cause of the surface specificity of the VSF spectral response under the dipole approximation. The damping term, γ, was treated as an empirical parameter held fixed at 2 cm^{-1}. The modifications to the MH technique include a dipole−dipole interaction for intermolecular OH bonds that exhibit favorable geometric coordination and a variable intramolecular coupling constant dependent upon the degree of solvation for a given water molecule.[41]

The local field correction, $F_{SFG} f_{VIS} f_{IR}$, was defined here as the product of Fresnel coefficients[42] and unit polarization vectors for the linear incident visible (f_{VIS}) and infrared (f_{IR}) beams along with the nonlinear detected sum frequency signal (F_{SFG}). The maximum value from the dispersion of water[43] (within the frequency range of 2800−3800 cm^{-1}) was used for its refractive index, constant refractive indexes were used for CCl_4 (n_{CCl_4} = 1.460) and DCE (n_{DCE} = 1.445), and the refractive index of the interface was treated as an average of the two bulk liquid values for every liquid−liquid system. The beam angles representative of the unit polarization vectors were calculated based upon the total internal reflection (TIR) geometry used in the experiments, and all values were held fixed throughout these experiments.[13] (A more accurate method of determining the sum frequency beam angle would involve applying the phase matching condition,[42] but a photomultiplier tube (PMT), whose angle was held fixed throughout these experiments, was used to efficiently detect the sum frequency signal.) As a result, the refractive indexes of the organic phase and the interfacial region were the only variable quantities throughout each set of liquid−liquid experiments applied in the local field correction.

Molecules were considered to be hydrogen bonded if their intermolecular OH bond separation was ≤2.5 Å and the

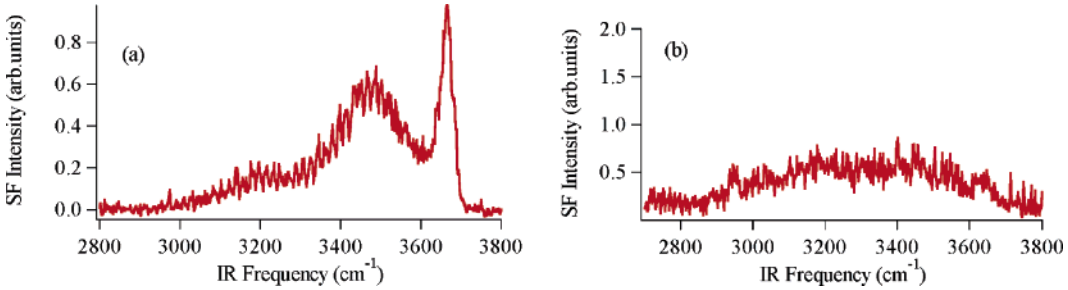

Figure 1. Experimental VSF spectra of (a) CCl_4-H_2O and (b) DCE$-H_2O$ interfaces in SSP polarization.

corresponding bond angle was ≤30°. These types of bonds were treated with the dipole−dipole coupling mentioned above and were labeled as "normal" hydrogen bonds. However, water molecules that exhibit this type of bonding alone do not reconstruct the entire VSF spectrum, so bonds that did not satisfy the angle requirement were also identified and labeled as "broken" hydrogen bonds, and together with normal hydrogen bonds the entire VSF spectrum of water could be reproduced. It should be noted that the correlation between the length of an intermolecular hydrogen bond and its vibrational frequency is poor,[44] but in this work normal hydrogen bonds are considered to be geometrically favored over broken hydrogen bonds due to the satisfaction of the angle requirement.

The naming scheme deployed by Buch[45] was adapted here as in previous vapor−water studies[41] to identify different types of water molecules based upon degree of hydrogen bonding. Hydrogen bonds located on the hydrogen atom (proton donors) were designated as "H-bonded" moieties, while those located on the oxygen atom (proton acceptors) were designated as "O-bonded" moieties. For example, a tetrahedrally coordinated water molecule was referred to as an OOHH-bonded water molecule whereas a water molecule that interacts as a single proton donor and single proton acceptor was designated as an OH-bonded species. As an addition to this notation, molecules that possess entirely normal hydrogen bonds (satisfying both distance and angle requirements) are given the prefix "*n*-", while those that possess partially or entirely broken hydrogen bonds are given the prefix "*b*-". With this notation, water molecules that possess one normal proton donor bond and one normal proton acceptor bond are identified as "*n*-OH-bonded" molecules, molecules that possess tetrahedral coordination where some or all of those bonds are broken are identified as "*b*-OOHH-bonded" molecules, and molecules identified without the "*n*-" or "*b*-" prefix represent the sum of both normal and broken types of water molecule. Molecules that possess no intermolecular hydrogen bonds are referred to as water monomers. Only the four closest intermolecular hydrogen bonds per molecule are considered for characterization.

Water molecules with one OH oscillator bound to a neighboring water molecule via its hydrogen atom and the other oscillator unbound via the hydrogen atom possess distinctly different vibrational frequencies and are often described as uncoupled because of the difference in energy between the two oscillators. The unbound OH oscillator is commonly referred to in the literature as a "free OH mode", and is typically easy to identify in experimental VSF spectra as a sharp peak near 3700 cm^{-1}. The bound OH oscillator is referred to as a "donor OH mode". In this computational work, these molecules fall into three categories because of their different possible bonding capabilities through the lone pairs on the oxygen atom (H-bonded, OH-bonded, and OOH-bonded molecules). The naming scheme described above was extended to these modes by placing the coordination label before the free/donor OH mode designation, i.e., *n*-OH-bonded donor OH mode. The "total free" OH mode label, without the bonding designation, was used to identify the sum of all free OH contributors, which is the nature of the mode most often identified in previous VSF experiments due to the inability to distinguish whether the molecule with this free OH mode is H-bonded, OH-bonded, or OOH-bonded to adjacent water molecules.

With the molecular hyperpolarizabilities available via the modified MH approach, they may be projected into the laboratory frame and binned according to frequency to create the macroscopic susceptibility, $\chi^{(2)}_{ijk} = N\langle\beta_{ijk}\rangle$ (see eqs 1 and 2 above). In order to compare the macroscopic susceptibility with the spectral response collected under typical VSF experiments, the nonresonant susceptibility ($\chi^{(2)}_{NR}$) and the local field correction ($F_{SFG}f_{VIS}f_{IR}$, described above) need to be accounted for. Unlike vapor−water studies,[46] a nonresonant contribution was not observed experimentally in any of the liquid−liquid systems studied in this paper, so that term was therefore neglected. All the spectral results described in this work are for SSP polarization, which probes IR transitions of OH stretch modes that oscillate perpendicular to the surface.

Results and Discussion

Modeling the (CCl_4 + DCE)$-H_2O$ Concentration Series. Figure 1a shows the experimental VSF results reported in earlier studies of the CCl_4-H_2O interface.[12,31] The most easily identifiable feature is the free OH peak at 3670 cm^{-1} that corresponds to the OH bond of interfacial water that points into the organic phase. This peak is slightly red-shifted compared to that found at the vapor−water interface, indicative of weak bonding interactions between CCl_4 and the free OH bond of water that has one bond in the organic phase and the corresponding donor OH bond hydrogen bonded to nearby water molecules. The intensity at lower frequencies is comprised of several contributions previously discussed.[12,31] The major contributor to the spectrum is the response from the companion donor OH mode that is energetically uncoupled from its adjacent free OH mode. The experimental identification of the frequency of the donor OH mode (with unspecified degrees of OH, OOH, and H bonding) was enabled by means of isotopic dilution (HOD/D_2O) experiments.[31] The donor OH contribution is found to be particularly strong in the SSP response, as is the case with the free OH bond, due to both large interfacial populations and strong orientation preferences.[41] Other experimental contributions from more solvated species are found at lower frequencies. Near the free OH mode, small contributions from water molecules that penetrate into the CCl_4 phase and orient with their hydrogen atoms toward bulk CCl_4 are also found. Overall, the spectral response of this liquid−liquid system is similar to the resonant spectrum of the vapor−water interface.[46]

In contrast, Figure 1b shows the VSF spectrum of the DCE$-H_2O$ interface. This spectrum is relatively featureless compared

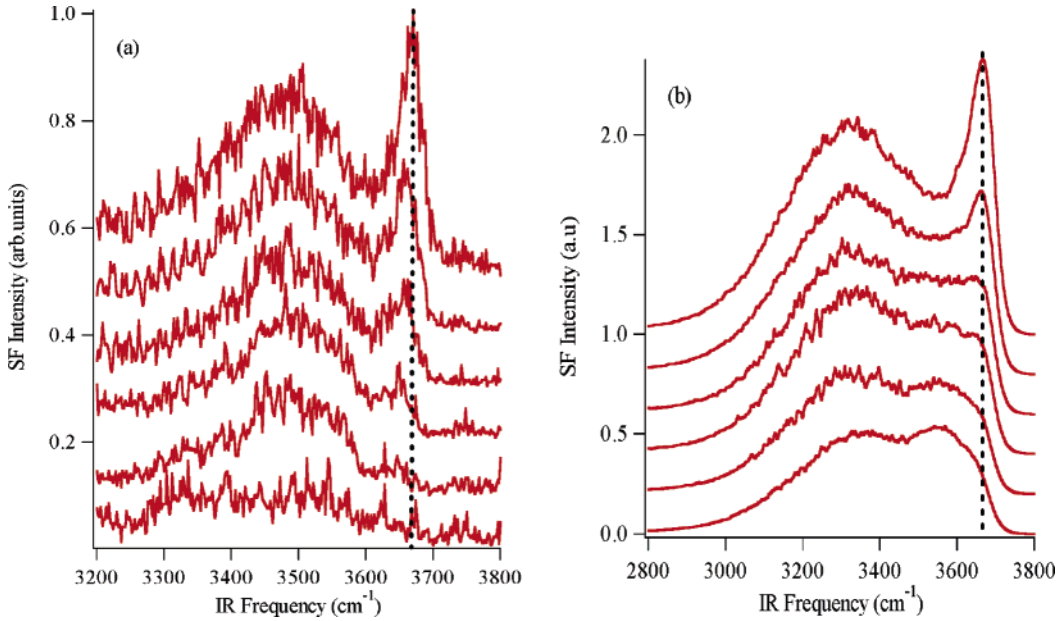

Figure 2. (a) Experimental and (b) computational concentration series of the (CCl_4 + DCE)−H_2O interface. Each series ranges from neat CCl_4−H_2O (top) to neat DCE−H_2O (bottom) in concentration. Spectra have been shifted on the *y*-axis for clarity, and a dashed black line has been added to aid in the identification of the small red shift in the total free OH peak.

to that of the CCl_4−H_2O interface (Figure 1a) and possesses a low signal throughout the entire OH stretch region. In order to assess what interfacial molecular structure and bonding of water is responsible for the spectral differences between these systems, a series of liquid−liquid experiments were devised where the organic phase consisted of CCl_4 and DCE mixtures of various concentrations. Figure 2a shows that, as the quantity of DCE increases, the spectral line shape progresses from that of a neat CCl_4−H_2O system to that of a neat DCE−H_2O system. This progression consists of a small red shift and broadening of the free OH peak at 3670 cm^{-1} and its eventual merging with the broader response at lower frequencies. This is accompanied by an overall reduction in signal throughout the OH stretch region.

Since the concentration series shown in Figure 2a contains local field effects, the modeling of this series requires adding local field effects to the computational result. In doing so, the refractive index for the organic mixtures was simply approximated as an average value based on organic liquid composition. (Surface pressure experiments conducted by this laboratory show DCE is surface active when mixed with CCl_4 at the (CCl_4 + DCE)−H_2O interface, so the refractive index for the organic mixture is *not* expected to follow a linear progression at the surface.[13]) The computational concentration series of the (CCl_4 + DCE)−H_2O interface is shown in Figure 2b. The computational result reproduces the eventual disappearance of the 3670 cm^{-1} mode and reasonably reproduces the overall loss of spectral intensity as the DCE concentration increases. Given the relatively good correspondence between the calculated and experimental spectra, detailed information can be extracted about the population density, coordination, and orientation of various constituent OH stretch modes that are embedded in these spectral calculations.

Density Profiles of CCl_4−H_2O and DCE−H_2O Interfaces. The number of molecules for any given liquid is configured to achieve their densities in bulk solution. At 0.997 g/mL, the fractional compositions of different species of water approximately represent percentages of total density. Figure 3a shows density profiles for the CCl_4−H_2O (solid lines) and DCE−H_2O (dashed lines) systems along the entire periodic cell. The horizontal axis represents the *z*-coordinate, which is the

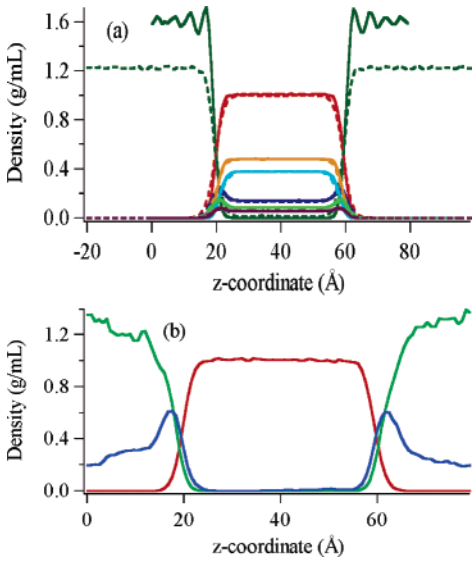

Figure 3. (a) Density profiles for CCl_4−H_2O (solid) and DCE−H_2O (dashed) interfaces. Dark green, total organic; red, total water; orange, OHH-bonded water; light blue, OOHH-bonded water; dark blue, total free water; light green, OH-bonded water; purple, OOH-bonded water. (b) Density profile of the (CCl_4 + DCE)−H_2O interface at 30% DCE (v/v). Green, CCl_4; blue, DCE; red, H_2O.

axis normal to the interfacial plane. Values of the *z*-coordinate from $z < 0$ Å and $z > 80$ Å are representative of the DCE phase, which is treated as a reservoir for water molecules and is not used to collect statistical information for water, thus making the region 0 Å $< z <$ 80 Å the only region used for data collection for both systems. Shown within this region are profiles of the total water densities and dominant water moieties, in addition to profiles of the two organic liquids. The DCE density profile remains smooth as it approaches the interface while that of CCl_4 appears oscillatory—this is representative of the layered packing of CCl_4 at the water surface.[47]

Figure 3b shows the density profile of the (CCl_4 + DCE)−H_2O interface at 30% DCE composition (v/v). In accordance with earlier surface pressure measurements,[13] the density profile of this mixed organic concentration shows that the increased

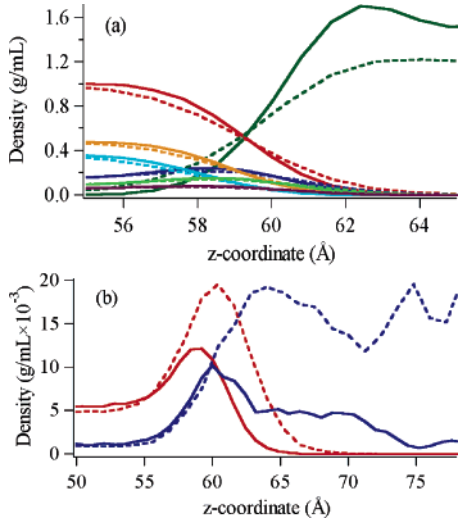

Figure 4. (a) Magnified schematic of interfacial profiles for the CCl_4-H_2O (solid) and DCE$-H_2O$ (dashed) interfaces featured in Figure 3a. Dark green, total organic; red, total water; orange, OHH-bonded water; light blue, OOHH-bonded water; dark blue, total free water; light green, OH-bonded water; purple, OOH-bonded water. (b) Density profiles for OO-bonded (red) and monomer (blue) molecules at the CCl_4-H_2O (solid) and DCE$-H_2O$ (dashed) interfaces. Water monomer profiles are scaled by 20× to fit the graph.

surface affinity of DCE compared to CCl_4 leads to a higher DCE density at the interface than that which exists in the bulk of the mixed organic phase. The density of CCl_4 is correspondingly smaller at the interface than in the bulk of the organic mixture. Theoretical studies of the dihedral conformation of DCE reveal these molecules prefer gauche formations when placed against the water surface.[2] This conformational acquisition of a dipole moment enables DCE to become more stable at the water surface than CCl_4, which remains nonpolar. This trend in density is also found for other organic mixtures shown in Figure 2b.

Figure 4a provides a more detailed picture of the interfacial regions of Figure 3a. This figure provides a comparison of the density profiles for different contributing water moieties at the DCE$-H_2O$ and CCl_4-H_2O interfaces within a 10 Å region that surrounds the interface. The interfacial thicknesses are approximately 8 and 6 Å for water in DCE and in CCl_4, respectively, consistent with other experimental and computational studies.[3,48] Also observed is a greater degree of penetration of DCE into the aqueous phase relative to CCl_4, consistent with a wider interfacial region. Of the individual types of water molecules, the OHH-bonded and OOHH-bonded water populations follow the behavior of their respective total water profiles, decreasing in population more rapidly within the water-rich portion of the DCE$-H_2O$ interfacial region than the CCl_4-H_2O system, and extending deeper into the DCE-rich phase than the CCl_4-rich phase. Unlike the profiles of OHH-bonded and OOHH-bonded molecules, the total free population peaks in concentration within the interfacial region. The total free profile (density profile of all water molecules containing free OH oscillators) consists of H-bonded (1%), OH-bonded (65%), and OOH-bonded (34%) water molecules. Its population possesses a slightly higher peak value for the CCl_4-H_2O system (0.24 g/mL) relative to the DCE$-H_2O$ system (0.21 g/mL), but in a manner similar to that of other water profiles, the total free profile extends deeper into the DCE-rich portion of the interfacial region compared to that of CCl_4. The overall picture created between these two interfacial systems is one where the interfacial thickness of the DCE$-H_2O$ system is wider than that of CCl_4-H_2O, and the largest types of water populations are also extended over a wider interfacial range for the DCE$-H_2O$ system compared to the CCl_4-H_2O system.

Figure 4b shows density profiles for OO-bonded water molecules and water monomers for the two systems. In this work, OO-bonded molecules comprise the sum of O-bonded and OO-bonded species. The values of the *z*-coordinate are the same here as they are within Figure 4a, so the interfacial region lies approximately from 55 to 65 Å, with the bulk water region lying at lower values and the bulk organic region lying at larger values. Within the bulk water region closest to the interface, OO-bonded molecules possess negligibly lower populations in the DCE$-H_2O$ system than in the CCl_4-H_2O system, but within the interfacial region that trend is dramatically reversed. There is a significantly greater population of OO-bonded molecules in the DCE$-H_2O$ system, and this larger peak population also extends deeper into the DCE-rich region compared to the CCl_4 system. The density profile of water monomers (water molecules with no hydrogen bonding to other water molecules) also shows a dramatic increase in peak population in the DCE phase compared to the CCl_4 phase and, unlike its profile at the CCl_4-H_2O interface, continues to persist in population more than 10 Å beyond the interface into the DCE phase. This is consistent with the higher solubility of water in DCE relative to CCl_4. The prevalence of OO-bonded molecules and water monomers is consistent with the experimental VSF spectral result for the CCl_4-H_2O interface where OO-bonded molecules and water monomers were shown to be present in the interfacial region.[31] However, their increased populations at the DCE$-H_2O$ interface suggests that they may play an even more important role in the VSF spectral response for that interface than for the CCl_4-H_2O interface.

Orientation Distributions of Water at the CCl_4-H_2O and DCE$-H_2O$ Interfaces. Tilt angle distributions were collected for the different OH bond oscillators. Angles are measured relative to the positive *z*-axis (normal to the surface and extending into the organic phase), so angles within the range $0 < \theta < 90°$ are described as being "above" the plane of the interface (toward the organic phase) whereas angles within the range $90° < \theta < 180°$ are "below" the plane of the interface (toward the water phase). To allow greater emphasis on interfacial distributions, 30 Å of bulk water was excluded from data collection. Since the tilt angle of one OH oscillator was measured independently of the other, no immediate correlations can be made between them. Each distribution was also normalized by $\sin\theta$, causing an isotropic distribution of angles to appear as a flat profile. Under the dipole approximation, only OH oscillators that possess net orientation (above or below the plane of the interface) will contribute to VSF intensity.

Figure 5a shows the tilt angle distributions for OH-bonded water molecules at the CCl_4-H_2O (red) and DCE$-H_2O$ (blue) interfaces. These OH-bonded water molecules possess free OH and donor OH oscillators and clearly show tilt angle preferences for these bonds above and below the interface, respectively. Comparing their distributions between the two interfacial systems, the orientation of the OH-bonded free OH oscillator shows a slightly stronger angle preference toward the organic phase in the DCE$-H_2O$ system compared to the CCl_4-H_2O system, while that of the OH-bonded donor OH oscillator is found to be similar for both systems.

Figure 5b shows tilt angle distributions for OOH-bonded water molecules, which also possess free OH and donor OH oscillators. Both the OOH-bonded free OH oscillator and OOH-

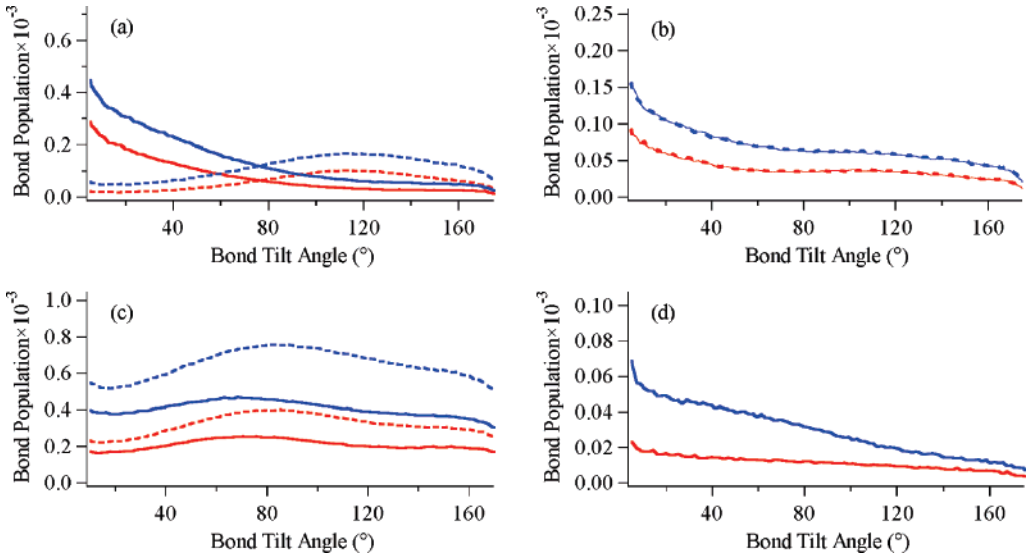

Figure 5. Tilt angle distributions for various water species at the CCl_4-H_2O (red) and DCE$-H_2O$ (blue) interfaces. (a) OH-bonded free (solid) and OH-bonded donor (dashed) water. (b) OOH-bonded free (solid) and OOH-bonded donor (dashed) water. These distributions overlap entirely. (c) OOHH-bonded (solid) and OHH-bonded (dashed) water. (d) OO-bonded water.

bonded donor OH oscillator tilt angle distributions differ significantly from their OH-bonded equivalents at both interfaces. The OOH-bonded free OH and OOH-bonded donor OH tilt angle distributions are very broad, with directional preference above the plane of the interface toward the organic phase for *both* OH oscillators in both systems. The angle preference for both OH oscillators toward the organic phase appears to be slightly greater at the DCE$-H_2O$ interface compared to the CCl_4-H_2O interface. The fact that both OH oscillators for OOH-bonded water molecules prefer to point toward the organic phase suggests that the main driving force behind their orientation preference at the interface is likely due to the formation of hydrogen bonds to other water molecules through the two lone pairs.

Figure 5c shows tilt angle distributions for OHH-bonded (dashed lines) and OOHH-bonded (solid lines) water molecules at the CCl_4-H_2O (red) and DCE$-H_2O$ (blue) interfaces. For these molecules, the angle distributions for the individual OH oscillators overlap completely, so each profile represents the angle distributions for both oscillators. In brief, OHH-bonded molecules tend to orient their OH oscillators almost parallel to the interface with a slight angular preference for their OH oscillators toward the water phase. The OOHH-bonded molecules also tend to orient their OH oscillators almost parallel to the interface and have slightly broader distributions. Both sets of distributions show slightly more preference toward the water phase at the DCE$-H_2O$ interface compared to the CCl_4-H_2O interface.

Figure 5d shows tilt angle distributions for OO-bonded water molecules. The angle distributions of the individual OH oscillators overlap completely, so each profile represents the angle distributions for both oscillators. These distributions show that the effect of organic liquid polarity on these types of molecules is significant. The tilt angle distributions for OO-bonded molecules in both systems show orientation preferences with hydrogen atoms pointed toward the organic phase. This preferential alignment of OO-bonded molecules at the DCE$-H_2O$ interface is significantly greater than that at the CCl_4-H_2O interface. Although no direct correspondence between the individual OH oscillators can be made, the dominance of OH oscillator preference for smaller angles at the DCE$-H_2O$ interface suggests the entire OO-bonded molecule is being oriented with both OH oscillators simultaneously directed toward the organic phase.

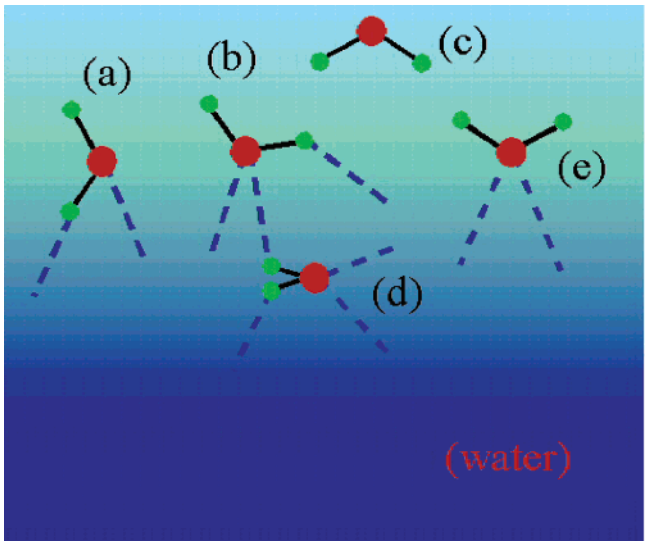

Figure 6. Orientations of interfacial water molecules as determined from tilt angle distributions. Dashed lines indicate intermolecular hydrogen bonds. (a) OH-bonded molecules; (b) OOH-bonded molecules; (c) water monomers; (d) OOHH-bonded molecules; (e) OO-bonded molecules.

Tilt angle distributions of H-bonded molecules and water monomers (no bonding to other water molecules) were also obtained and will be briefly discussed. H-bonded free OH and H-bonded donor OH oscillators show clear tilt angle preferences toward the organic and water phases respectively in both systems. Both types of OH oscillators (H-bonded free OH and H-bonded donor OH) show greater preference for smaller tilt angles within the DCE$-H_2O$ system compared to the CCl_4-H_2O system. Water monomers show tilt angle preferences of both their OH oscillators toward the water phase within both the DCE$-H_2O$ and CCl_4-H_2O systems, suggesting a molecular orientation that results in both hydrogen atoms simultaneously pointed toward the bulk water phase. Figure 6 shows a graphical representation of the molecular orientations of different types of interfacial water molecules as indicated by their tilt angle distributions.

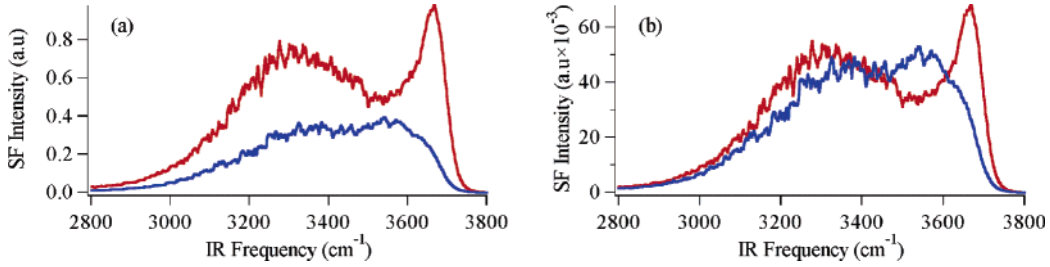

Figure 7. Computational VSF spectra of the CCl_4-H_2O (red) and DCE$-H_2O$ (blue) interfaces with (a) local field effects included and (b) local field effects removed.

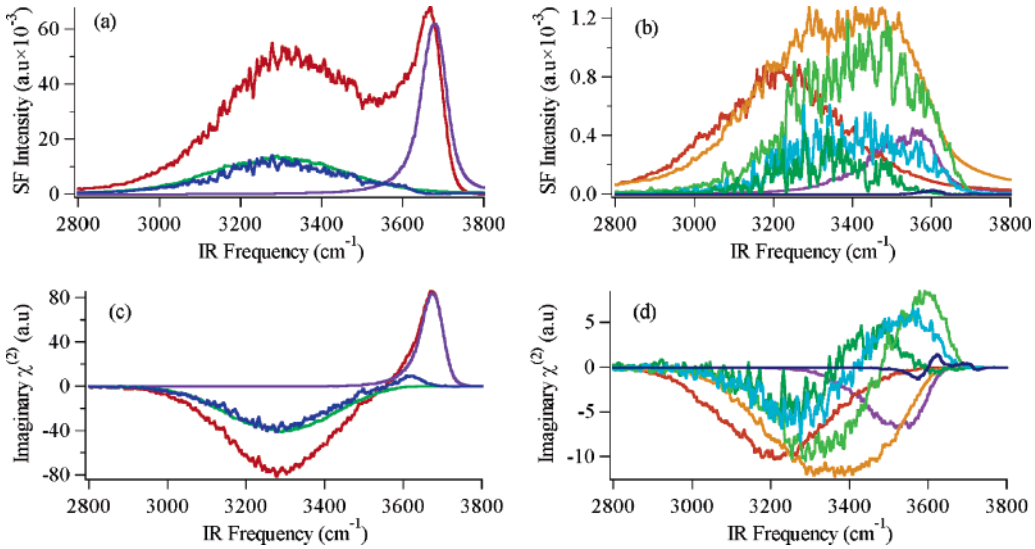

Figure 8. Computational (a) VSF spectra and (c) imaginary susceptibilities of the CCl_4-H_2O interface with contributions from the most intense OH stretch modes. Red, total spectrum; purple, total free OH; green, *n*-OH-bonded donor OH; blue, all other modes combined. Computational (b) VSF spectra and (d) imaginary susceptibilities from the next most intense set of OH stretch modes at the CCl_4-H_2O interface. Light orange, *b*-OOH-bonded; dark orange, *n*-OOH-bonded; light green, *b*-OHH-bonded; light blue, *b*-OOHH-bonded; dark green, *n*-OHH-bonded; purple, *b*-OH-bonded; dark blue, OO-bonded (approximately 3600 cm^{-1}).

Overall, the knowledge obtained from tilt angle distributions and density profiles provides a clearer picture of the types of water molecules dominant in the VSF spectra of the DCE$-H_2O$ and CCl_4-H_2O interfaces. For water molecules that possess free OH and donor OH oscillators, OH-bonded water molecules possess greater populations and more distinct tilt angle preferences for their free OH oscillators (toward the organic phase) and donor OH oscillators (toward the water phase) compared to those of OOH-bonded water molecules. Consequentially, the VSF response from OH-bonded molecules is expected to be greater than those of OOH-bonded molecules in SSP polarization for both interfacial systems. For water molecules that are more heavily solvated, OHH-bonded molecules possess greater populations at the interface than OOHH-bonded molecules along with a slight tilt angle preference. As a result, the VSF response from OHH-bonded molecules should be greater than that of OOHH-bonded molecules in SSP polarization for both interfacial systems. When comparing interfacial systems, OO-bonded molecules show stronger tilt angle preferences of their OH oscillators toward the organic phase at the DCE$-H_2O$ interface compared to the CCl_4-H_2O interface. This combined with their larger population would result in a larger VSF response from OO-bonded molecules in the DCE$-H_2O$ interface compared to the CCl_4-H_2O interface. H-bonded molecules and water monomers also show favorable tilt angle distributions for contributing spectral intensity in SSP polarization, but given their low densities, they should have less of a contribution to the VSF response, particularly for the CCl_4-H_2O interface. These types of observations will be discussed in greater detail below when the VSF spectra for CCl_4-H_2O and DCE$-H_2O$ are deconvoluted.

Computational Deconvolution of CCl_4-H_2O and DCE$-H_2O$ VSF Spectra. Figure 7a shows computational VSF spectra of the CCl_4-H_2O (red) and DCE$-H_2O$ (blue) interfaces. These spectra include local field effects and most closely resemble the VSF spectra that are obtained experimentally for these systems. Figure 7b shows the same computational spectra with the local field effects removed. When field effects are removed, the magnitude of the VSF intensity for the DCE$-H_2O$ interface becomes comparable to that of the CCl_4-H_2O interface across the entire OH stretching region. The spectra in Figure 7b represent the square of *actual* macroscopic susceptibilities ($\chi^{(2)}_{ijk} = N\langle\beta_{ijk}\rangle$), as opposed to the *effective* susceptibilities ($F_{SFG}f_{VIS}f_{IR}N\langle\beta_{ijk}\rangle$) shown in Figure 7a. It is the deconvolution of the spectra in Figure 7b that will allow for an accurate description of the interfacial water environment for each system.

The deconvolution of the CCl_4-H_2O interface is shown in Figure 8. Figure 8a,b shows the VSF intensities of deconvoluted OH stretch modes, a useful representation for the comparison of spectral contributions with experiments; Figure 8c,d shows their corresponding imaginary susceptibilities, a useful representation for identifying the phase relationships between these deconvoluted OH stretch modes that are not identifiable using VSF intensities. Figure 8a shows that the total free OH mode obtained computationally peaks at 3670 cm^{-1}, in good agreement with experimental observations for this interfacial system.[12,31] Also shown is the *n*-OH-bonded donor OH mode that dominates the entire hydrogen-bonded region, also in good

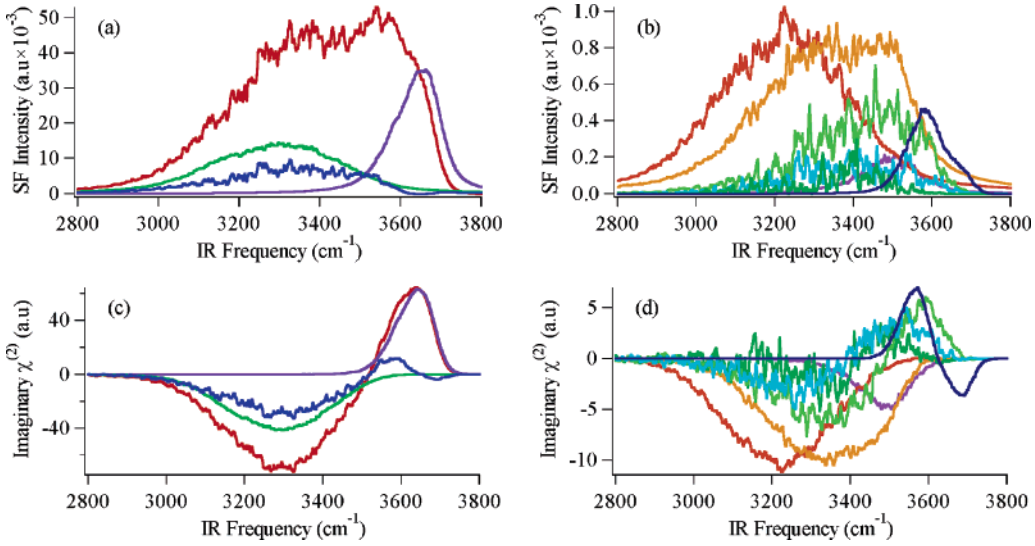

Figure 9. Computational (a) VSF spectra and (c) imaginary susceptibilities of the DCE−H_2O interface with contributions from the most intense OH stretch modes. Red, total spectrum; purple, total free OH; green, *n*-OH-bonded donor OH; blue, all other modes combined. Computational (b) VSF spectra and (d) imaginary susceptibilities from the next most intense set of OH stretch modes at the DCE−H_2O interface. Light orange, *b*-OOH-bonded; dark orange, *n*-OOH-bonded; light green, *b*-OHH-bonded; light blue, *b*-OOHH-bonded; dark green, *n*-OHH-bonded; purple, *b*-OH-bonded; dark blue, OO-bonded.

agreement with the assignment of the donor OH mode revealed by isotopic dilution experiments to be the major contributor within the hydrogen-bonding region.[31] This donor OH mode possesses a spectral intensity slightly larger than the collective contributions of all other OH stretch modes. Figure 8b shows contributions from the next largest set of OH stretch modes that contribute to the collective peak displayed in Figure 8a. Generally speaking, these modes are broad, asymmetric, and contain a large degree of overlap with other OH stretch modes of similar frequency but different molecular environments. The dominant OH stretch modes in this smaller contributing set are primarily from OOH-bonded water molecules and OHH-bonded water molecules. Contributions from *b*-OOHH-bonded and *b*-OH-bonded water are also present. Within this set of OH stretch modes, molecules that exhibit *b*-bonding dominate the spectral region above 3200 cm^{-1}, with *b*-bonding molecules comprising the four largest spectral contributors above 3450 cm^{-1}. Barely visible is the spectral contribution from OO-bonded molecules. Upon closer inspection, the peaks from OO-bonded molecules appear at 3605 and 3710 cm^{-1}, which is in good agreement with experimental results.[31] Within the scale of Figure 8b, the spectral contributions from the H-bonded donor OH mode and water monomers are negligibly small, indicative of their low densities. Figure 8c,d shows that the OH stretch region acquires a predominantly negative phase at lower frequencies and a positive phase at higher vibrational frequencies. This is consistent with the overall phase relationship identified at the vapor−water interface from both experiments[46] and simulations,[40] suggesting that their molecular environments are very similar.

The deconvolution of the DCE−H_2O interface is shown in Figure 9. Figure 9a,b shows VSF intensities of deconvoluted OH stretch modes, while Figure 9c,d shows their corresponding imaginary susceptibilities. Unlike that of the CCl_4−H_2O interface, the experimental spectrum for this system could not be deconvoluted into its constituent OH stretch modes using standard curve fitting routines, due to the loss of distinct spectral features in addition to the lack of spectral intensity overall. Isotopic dilution studies have not been conducted on this system as they have been for CCl_4−H_2O. Figure 9a shows that the spectral intensity of the total free OH mode dominates over all other OH stretch modes, even though there is no distinct free OH peak in the overall spectrum. Compared to that of the CCl_4−H_2O system, the total free OH mode is lower in peak intensity and is asymmetrically broadened to the red due to stronger H_2O−DCE interactions than H_2O−CCl_4 interactions. This red shift was observable experimentally within the (CCl_4 + DCE)−H_2O concentration series, and a quadratic extrapolation of that series estimates the free OH mode for the neat DCE−H_2O system to be near 3630 cm^{-1}.[13] The uncoupled OH stretch mode of HOD dissolved in DCE was observed at 3635 cm^{-1}.[49] The total free OH mode shown in Figure 9a possesses a slightly higher peak frequency at 3650 cm^{-1}. Figure 9a also shows that the *n*-OH-bonded donor OH mode dominates over the collective contributions from other hydrogen-bonded OH stretch modes, but in this system the degree of dominance is even greater. In comparison to the CCl_4−H_2O interface (see Figure 8a), the *n*-OH-bonded donor OH mode is of comparable intensity between the two interfacial systems, while the peak that describes the collective contributions from all other OH stretch modes is of lower intensity. Figure 9b shows the OH stretch modes that contribute to the collective peak in Figure 9a. Comparing the OH stretch modes in Figure 9b from the DCE−H_2O interface to the equivalent set of OH stretch modes from the CCl_4−H_2O interface (see Figure 8b), the peaks from the *n*-OOH-bonded donor OH mode and *n*-OHH-bonded water molecules are of comparable intensities, while all the OH stretch modes with *b*-bonding are reduced in spectral intensity. Compared to the CCl_4−H_2O interface (Figure 8b) where molecules exhibiting *b*-bonding dominate that set of OH stretch modes above 3200 cm^{-1}, *b*-bonded water molecules at the DCE−H_2O interface (Figure 9b) dominate this set of OH stretch modes between 3300 and 3550 cm^{-1}, with only the *b*-OOH-bonded donor OH mode and *b*-OHH-bonded water molecules dominating other OH stretch modes from approximately 3430 to 3500 cm^{-1}. The spectral contribution from OO-bonded water molecules is substantially greater in the DCE−H_2O spectrum compared to that observed in the CCl_4−H_2O spectrum. Within the scale of Figure 9b for the DCE−H_2O system, spectral contributions from the H-bonded donor OH mode and from water monomers are small, despite the increased concentration of water monomers throughout the organic phase. Similar to

Figure 8c,d, Figure 9c,d shows that the phase of the imaginary susceptibilities at the DCE$-H_2O$ interface acquires negative values at lower frequencies and positive values at higher frequencies. The loss of a distinct peak corresponding to the total free OH mode (Figure 9a) can be understood using Figure 9c. In Figure 9c, the interference between the total free OH mode and the peak representing the collective contributions from other OH stretch modes is constructive around 3600 cm^{-1}, resulting in an accumulation of VSF intensity that far exceeds that of the total free OH mode. (This effect is also observed at the CCl_4-H_2O interface, but to a much lesser degree.) The collective peak shown in Figure 9c is deconvoluted in Figure 9d. Deconvolution of this collective peak shows that the accumulation of constructive interference is attributed to OO-bonded molecules, whose VSF intensity is significantly greater at the DCE$-H_2O$ interface compared to the CCl_4-H_2O interface.

The overall picture created by the spectral deconvolution of the DCE$-H_2O$ interface is one of stronger interactions between DCE and H_2O relative to CCl_4 and H_2O. These stronger interactions manifest themselves in (1) a red-shifted, broadened total free OH peak that merges with contributions from hydrogen-bonded OH stretch modes, (2) increased alignment and spectral contribution from OO-bonded molecules that contribute intensity to the higher frequency region, and (3) a loss of intensity by *b*-bonded water molecules that exhibit geometrically unfavorable hydrogen bonding compared to their *n*-bonded equivalents. The net effect of these changes results in a VSF spectrum that loses its distinct spectral features due to the combined spectral interferences of the total free OH mode, OO-bonded molecules, and *b*-bonded water molecules of high spectral frequency, necessitating the need for a more detailed approach toward its deconvolution.

It should be noted that local field effects also make a significant contribution to the reduced overall intensity at the DCE$-H_2O$ interface compared to the CCl_4-H_2O interface. These effects need to be accounted for to accurately compare the experimental spectral response with the corresponding computational spectrum generated from MD simulations. The CCl_4-H_2O VSF spectrum is in good agreement between the experimental and computational approaches. The computational and experimental agreement for the DCE$-H_2O$ VSF spectrum, however, can be improved, particularly at higher frequencies. Computationally, this improvement can come in the form of a more robust polarizable model for DCE—the agreement between the computational and experimental VSF spectra was found to correlate well with the degree of agreement between the computational free OH peak frequency and experimental estimates. Experimentally, weak DCE overtones are expected to result in a dispersion within the organic index of refraction, a factor that is not considered in this work as the organic index of refraction was treated with a constant value. Addressing these considerations may result in improved agreement between the computational and experimental spectra of the DCE$-H_2O$ interface.

Summary and Conclusions

Spectral calculations of the CCl_4-H_2O and DCE$-H_2O$ interfaces based on molecular dynamics simulation have been performed to better understand the structure of these interfacial systems. Unlike the CCl_4-H_2O VSF spectrum that contained distinct spectral features, thus enabling spectral deconvolution with established curve fitting routines, the featureless DCE$-H_2O$ VSF spectrum measured in previous studies could only be interpreted as a more randomly oriented interface. These studies show that in fact there is significant water orientation present at the DCE$-H_2O$ interface, but that additional molecular factors contribute to obscure this in the measured spectrum. The calculated results provide a detailed picture of the unique types of interfacial water moieties contributing to the DCE$-H_2O$ spectrum and the role of spectral broadening (in the total free OH peak), frequency shifting (by *b*-bonded water molecules), and spectral interferences in the overall measured spectrum (by oriented OO-bonded water molecules and a smaller contribution from water monomers).

The dominant contributor to the VSF intensities is found to be the same for both systems: These *n*-OH-bonded interfacial water molecules with their highly oriented free OH and corresponding donor OH bonds directed toward the organic and water bulk phases, respectively, possess peak concentrations at the interface. A significant population of OHH- and OOHH-bonded water species are also present at both the DCE$-H_2O$ and CCl_4-H_2O interfaces. The VSF signal from these molecules is small in SSP polarization because their orientation is largely parallel to the interface. In contrast to other liquid−liquid systems studied by VSF spectroscopy, the DCE$-H_2O$ interface has a larger population of oriented water monomers and oriented OO-bonded water molecules that penetrate further into the organic-rich interfacial region. There are also stronger perturbations within the water phase for water molecules that exhibit geometrically unfavorable hydrogen-bonding interactions. These calculations are consistent with the VSF experimental results in that these stronger DCE$-H_2O$ interactions lead to a wider interfacial region consisting of a variety of different DCE$-H_2O$ environments that make significant contributions to the spectral VSF intensity.[13]

VSF spectroscopy is routinely shown to be a powerful experimental technique capable of readily identifying small changes in the hydrogen-bonding network of the water surface. This is evident from studies of liquid−liquid systems involving nanomolar concentrations of surfactant,[10,11,17] to studies of the vapor−water interface using acids and salts,[50−52] and to the observations made in this work. In many of these studies, spectral fitting is a good first step in identifying different water species. However, these and similar calculations at the vapor−water interface[41] bring a much richer picture of the different types of contributing water species when combined and contrasted with VSF experimental results. Remarkable advances have been made in our understanding of hydrogen bonding in water due to a combined effort from both experimental and theoretical approaches. The goal of these computational studies and those of others is to eventually reach a convergence of experiment and theory in understanding the molecular structure of water and ice surfaces.

Acknowledgment. The authors would like to thank the National Science Foundation (CHE 0243856) and the Department of Energy, Office of Basic Energy Sciences, DE-FG-02-96ER4557.

References and Notes

(1) Pratt, L.; Pohorille, A. *Chem. Rev.* **2002**, *102*, 2671.
(2) Benjamin, I. *J. Chem. Phys.* **1992**, *97*, 1432.
(3) Benjamin, I. *J. Phys. Chem. B* **2005**, *109*, 13711.
(4) Schweighofer, K. J.; Benjamin, I. *J. Electroanal. Chem.* **1995**, *391*, 1.
(5) Dominguez, H.; Berkowitz, M. L. *J. Phys. Chem. B* **2000**, *104*, 5302.
(6) Jedlovszky, P.; Vincze, A.; Horvai, G. *J. Chem. Phys.* **2002**, *117*, 2271.

(7) Jedlovszky, P.; Vincze, A.; Horvai, G. *Phys. Chem. Chem. Phys.* **2004**, *6*, 1874.
(8) Senapati, S.; Berkowitz, M. L. *Phys. Rev. Lett.* **2001**, *87*, 176101.
(9) Dang, L. X. *J. Phys. Chem. B* **2001**, *105*, 804.
(10) Richmond, G. L. *Chem. Rev.* **2002**, *102*, 2693.
(11) Scatena, L. F.; Richmond, G. L. *J. Phys. Chem. B* **2004**, *108*, 12518.
(12) Brown, M. G.; Walker, D. S.; Raymond, E. A.; Richmond, G. L. *J. Phys. Chem. B* **2003**, *107*, 237.
(13) Walker, D. S.; Brown, M. G.; McFearin, C. L.; Richmond, G. L. *J. Phys. Chem. B* **2004**, *108*, 2111.
(14) Gragson, D. E.; Richmond, G. L. *J. Phys. Chem. B* **1998**, *102*, 3847.
(15) Du, Q.; Freysz, E.; Shen, Y. R. *Science* **1994**, *264*, 826.
(16) Leich, M. A.; Richmond, G. L. *Faraday Discuss.* **2005**, *129*, 1.
(17) Knock, M. M.; Bell, G. R.; Hill, E. K.; Turner, H. J.; Bain, C. D. *J. Phys. Chem. B* **2003**, *107*, 10801.
(18) Watry, M. R.; Richmond, G. L. *Langmuir* **2002**, *18*, 8881.
(19) Conboy, J. C.; Messmer, M. C.; Richmond, G. L. *Langmuir* **1998**, *14*, 6722.
(20) Watry, M. R.; Richmond, G. L. *J. Phys. Chem. B* **2002**, *106*, 12517.
(21) Walker, R. A.; Gruetzmacher, J. A.; Richmond, G. L. *J. Am. Chem. Soc.* **1998**, *120*, 6991.
(22) Smiley, B. L.; Richmond, G. L. *J. Phys. Chem. B* **1999**, *103*, 653.
(23) Tikhonov, A. M.; Mitrinovic, D. M.; Li, M.; Huang, Z.; Schlossman, M. L. *J. Phys. Chem. B* **2000**, *104*, 6336.
(24) Mitrinovic, D. M.; Zhang, Z.; Williams, S. M.; Huang, Z.; Schlossman, M. L. *J. Phys. Chem. B* **1999**, *103*, 1779.
(25) Schlossman, M. L. *Curr. Opin. Colloid Interface Sci.* **2002**, *7*, 235.
(26) Luo, G.; Malkova, S.; Pingali, S. V.; Schultz, D. G.; Lin, B.; Meron, M.; Benjamin, I.; Vanysek, P.; Schlossman, M. L. *J. Phys. Chem. B* **2006**, *110*, 4527.
(27) Wang, H.; Borguet, E.; Eisenthal, K. B. *J. Phys. Chem. B* **1998**, *102*, 4927.
(28) Steel, W. H.; Walker, R. A. *Nature* **2003**, *424*, 296.
(29) Steel, W. H.; Lau, Y. Y.; Beildeck, C. L.; Walker, R. A. *J. Phys. Chem. B* **2004**, *108*, 13370.
(30) Steel, W. H.; Walker, R. A. *J. Am. Chem. Soc.* **2003**, *125*, 1132.
(31) Scatena, L. F.; Richmond, G. L. *J. Phys. Chem. B* **2001**, *105*, 11240.
(32) Ishizaka, S.; Habuchi, S.; Kim, H.-B.; Kitamura, N. *Anal. Chem.* **1999**, *71*, 3382.
(33) Bain, C. D.; Davies, P. B.; Ong, T. H.; Ward, R. N.; Brown, M. A. *Langmuir* **1991**, *7*, 1563.
(34) Brown, M. G.; Raymond, E. A.; Allen, H.; Scatena, L. F.; Richmond, G. L. *J. Phys. Chem. A* **2000**, *104*, 10220.
(35) Case, D. A.; Pearlman, D. A.; Caldwell, J. W.; Cheatham III, T. E.; Wang, J.; Ross, W. S.; Simmerling, C. L.; Darden, T. A.; Merz, K. M.; Stanton, R. V.; Cheng, A. L.; Vincent, J. J.; Crowley, M.; Tsui, V.; Gohlke, H.; Radmer, R. J.; Duan, Y.; Pitera, J.; Massova, I.; Seibel, G. L.; Singh, U. C.; Weiner, P. K.; Kollman, P. A. University of California, San Francisco, 2002.
(36) Chang, T. M.; Peterson, K. A.; Dang, L. X. *J. Chem. Phys.* **1995**, *103*, 7502.
(37) Madurga, S.; Vilaseca, E. *J. Phys. Chem. A* **2004**, *108*, 8439.
(38) Chang, T. M.; Dang, L. X.; Peterson, K. A. *J. Phys. Chem. B* **1997**, *101*, 3413.
(39) Chang, T. M.; Dang, L. X. *J. Phys. Chem. B* **1997**, *101*, 10518.
(40) Morita, A.; Hynes, J. T. *Chem. Phys.* **2000**, *258*, 371.
(41) Walker, D. S.; Hore, D. K.; Richmond, G. L. *J. Phys. Chem. B* **2006**, *110*, 20451.
(42) Lobau, J.; Wolfrum, K. *J. Opt. Soc. Am. B* **1997**, *14*, 2505.
(43) Bertie, J. E.; Lan, Z. *Appl. Spectrosc.* **1996**, *50*, 1047.
(44) Moller, K. B.; Rey, R.; Hynes, J. T. *J. Phys. Chem. A* **2004**, *108*, 1275.
(45) Buch, V. *J. Phys. Chem. B* **2005**, *109*, 17771.
(46) Raymond, E. A.; Tarbuck, T. L.; Brown, M. G.; Richmond, G. L. *J. Phys. Chem. B* **2003**, *107*, 546−556.
(47) Hore, D. K.; Walker, D. S.; Richmond, G. L. *J. Am. Chem. Soc.* **2007**, *129*, 752.
(48) Strutwolf, J.; Barker, A. L.; Gonsalves, M.; Caruana, D. J.; Unwin, P. R.; Williams, D. E.; Webster, J. R. P. *J. Electroanal. Chem.* **2000**, *483*, 163.
(49) Jolicoeur, C.; Cabana, A. *Can. J. Chem.* **1968**, *46*, 567.
(50) Tarbuck, T. L.; Richmond, G. L. *J. Am. Chem. Soc.* **2006**, *128*, 3256.
(51) Mucha, M.; Frigato, T.; Levering, L. M.; Allen, H.; Tobias, D. J.; Dang, L. X.; Jungwirth, P. *J. Phys. Chem. B* **2005**, *109*, 7617.
(52) Raymond, E. A.; Richmond, G. L. *J. Phys. Chem. B* **2004**, *108*, 5051.